BREAK-UP TIME AND MORPHOLOGY OF DROPS AND BUBBLES IN A HIGH REYNOLDS NUMBER FLOW

Rodríguez-Rodríguez J, Gordillo JM, Martínez-Bazán C
Departamento de Ingeniería Térmica y de Fluidos
Universidad Carlos III de Madrid
Avda. de la Universidad 30, 28911, Leganés, Madrid, (SPAIN)

ABSTRACT

The break-up process of a drop or bubble immersed in a turbulent flow at high Reynolds numbers is numerically studied assuming that both the inner and the outer velocity fields are irrotational. Under this approximation, the time evolution of the drop's interface is computed, for a wide range of the inner to outer density ratio, Λ, through a boundary integral method once the turbulent velocity field is modelled as an axisymmetric straining potential flow. Despite of its simplicity, the model reproduces the main features of the turbulent break-up of drops and bubbles observed experimentally. Furthermore, if the density ratio is close to unity, the slender geometry of the drops observed in the numerical simulations suggest a simplified theoretical model which accurately reproduces the numerically obtained time evolution of the radius of the drop.

INTRODUCTION

Due to the complexity of turbulence, the study of the turbulent breakup of drops and bubbles (hereafter named particles) demands, as a first approach, simple models that retain the physical mechanisms of the breakup process. In the present paper, the turbulent breakup of particles at high Reynolds number is modelled assuming that both inner and outer velocity fields are irrotational. Furthermore, as suggested by the experimental results, the turbulent velocity fields which promote the breakup have been approximated, in the vicinity of the particle, to an axisymmetric straining flow. In effect, experiments on the breakup in a turbulent water jet of bubbles [1] or heptane droplets [2], show that the particles elongate in one direction during the first stages of the process (see Figs. 1a-b), giving rise to the so called cigar-shaped break-up [3]. Consequently, although the turbulent flow surrounding the particle is fully three dimensional and does not have any kind of symmetry, the flow pattern leading to the particle break-up can be modelled, in a first approximation, as an axisymmetric, hyperbolic type of flow (see [3]).

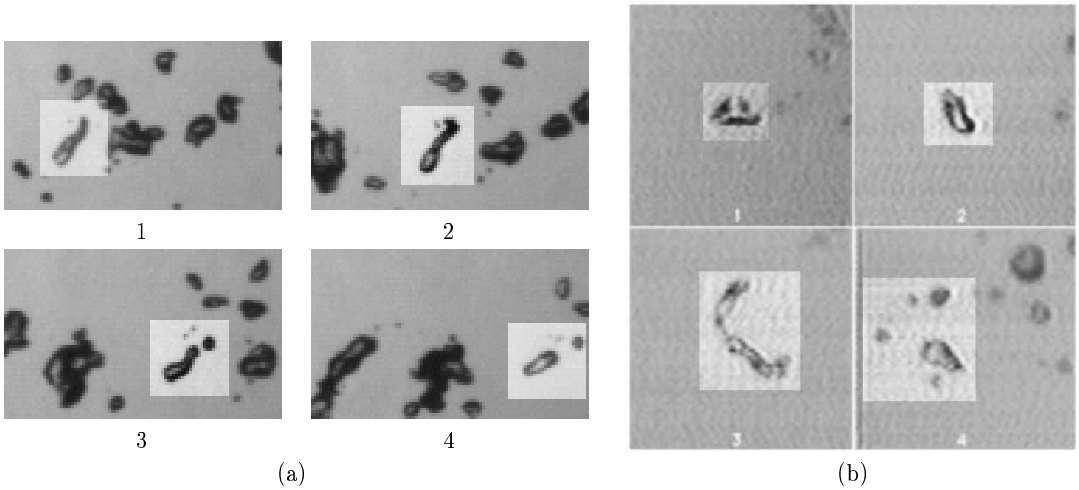

Fig. 1: (a) High speed (1000 f.p.s.) video images of the slender breakage of an air bubble injected at the centerline of a turbulent water jet. The flow goes from left to right. (b) Break-up of a heptane drop immersed in a turbulent water jet. It can be observed that the drop is stretched until it becomes a slender ligament before breaking. (Heptane images taken from [2]).

Although the present approach to model the external velocity field was first employed in the case of the axisymmetric viscous break-up of droplets, [4], the turbulent breakup of bubbles at high Reynolds numbers has also been studied by

Shreekumar et al. [5] and Higuera [6] under the same axisymmetric potential flow approximation for velocity fields different from the one adopted here.

The paper is structured as follows: the equations and boundary conditions governing the time evolution of the velocity and pressure fields, both inside and outside the particle, are described in the following section. Results concerning bubble and drop breakup will be also presented and the last section is devoted to the conclusions.

PROBLEM FORMULATION

The numerical simulations presented in this work provide with the time evolution of the interface of an immiscible particle of initial radius a_0 and density $\rho_{\rm i}$, immersed into an infinite volume of a different fluid of density $\rho_{\rm e}$, with a surface tension coefficient, σ. The flow inside and outside the droplet will be considered irrotational. The outer fluid velocity field far from the particle's interface is imposed and matches with a hyperbolic axisymmetric flow of the form

$$u_r = -2Mr/a_0 \ , \ u_z = 4Mz/a_0 \, , \tag{1}$$

where M is the flow intensity. In terms of the dimensionless variables defined with a_0, $t_c = \sqrt{\rho_{\rm e} a_0^3/\sigma}$ and $\rho_{\rm e}$ as the characteristic scales for length, time, and density respectively, the equations governing the inner and outer potential flows read

$$\nabla^2 \phi_{\rm (i,e)} = 0, \tag{2}$$

$$\Lambda_{\rm (i,e)} \left(\frac{\partial \phi_{\rm (i,e)}}{\partial t} + \frac{|\nabla \phi_{\rm (i,e)}|^2}{2} \right) + p_{\rm (i,e)} = P_{0\rm (i,e)}, \tag{3}$$

where the subscripts $\rm i, e$ stand for the inner and external fluid respectively. Equations (2) are the Laplace equations for the velocity potentials $\phi_{\rm (i,e)}$, and equations (3) are the Bernoulli equations for the pressure fields $p_{\rm (i,e)}$ with $\Lambda_{\rm (i,e)} = \rho_{\rm (i,e)}/\rho_e$. Moreover, $P_{0\rm (i,e)}$ are functions of time which, in this problem, can be set to zero without loss of generality since they can be included in the definitions of $\phi_{\rm (i,e)}$ without changing the velocity. Equations (2)-(3) must be solved subjected to the following boundary conditions

$$\frac{\partial \phi_{\rm (i,e)}}{\partial r} = 0 \qquad \text{at} \quad r = 0, \tag{4}$$

$$\nabla \phi_{\rm e} \rightarrow -\sqrt{We}\, r/4\, \mathbf{e_r} + \sqrt{We}\, z/2\, \mathbf{e_z} \qquad \text{when} \quad (r,z) \rightarrow \infty \tag{5}$$

and

$$p_{\rm i} - p_{\rm e} = \nabla \cdot \mathbf{n}_{\rm i}, \tag{6}$$

$$\frac{\partial \phi_{\rm i}}{\partial n_{\rm i}} = -\frac{\partial \phi_{\rm e}}{\partial n_{\rm e}}, \tag{7}$$

at the particle's interface. In equation (5), $We = \rho_e \left(8M\right)^2 a_0/\sigma$ is the particle's Weber number. The time evolution of the particle's interface will be computed by solving Eqs. (2-7) with the numerical method described in [7]. The results concerning the breakup of bubbles and drops are presented in the following two sections.

BUBBLE BREAK-UP

The first case of interest for practical applications is the break-up of a gas bubble immersed in a turbulent liquid flow. Since, in this case, the density ratio $\Lambda \ll 1$, the only parameter governing the problem is the Weber number. The time evolution of the bubble interface computed for two different values of the Weber number, namely $We = 3.0$ and $We = 10.0$, is depicted in Figs. 2a-b.

It must be noticed that, in the bubble break-up case, no satellites were formed and, therefore, the break-up was always binary within the range of Weber numbers explored $We_{\rm c} \leq We \leq 200$. Here $We_{\rm c}$ denotes the critical Weber number defined as the minimum value of We needed for a bubble to break. This conclusion is in agreement with previous experimental observations such those provided in [8, 9, 10, 1] who reported that the observed break-up events were mostly binary for moderately high Weber numbers. Bubble break-up leading to more than two fragments is rarely observed in experiments.

The numerical simulations also provide the dimensionless break-up time $T_{\rm b}$, shown in Fig. 3a for a wide range of Weber numbers. Notice that, in the limit of $We \gg 1$, the dimensionless break-up time scales as $T_{\rm b} \sim We^{-1/2}$, consistently with the fact that in this case the only relevant time scale of the problem is the convective time. Once an appropriate Weber number is defined, the results depicted in Fig. 3b may be used to compare with the experimentally measured frequency. Thus, our numerical results will be compared with the experimental measurements of the break-up time of air bubbles injected at the axis of a submerged turbulent water jet reported in [9, 10]. Since in these experiments the radius of the generated bubbles ($a_0 \simeq 0.89$ mm) falls within the inertial subrange of the turbulent energy spectrum, the flow

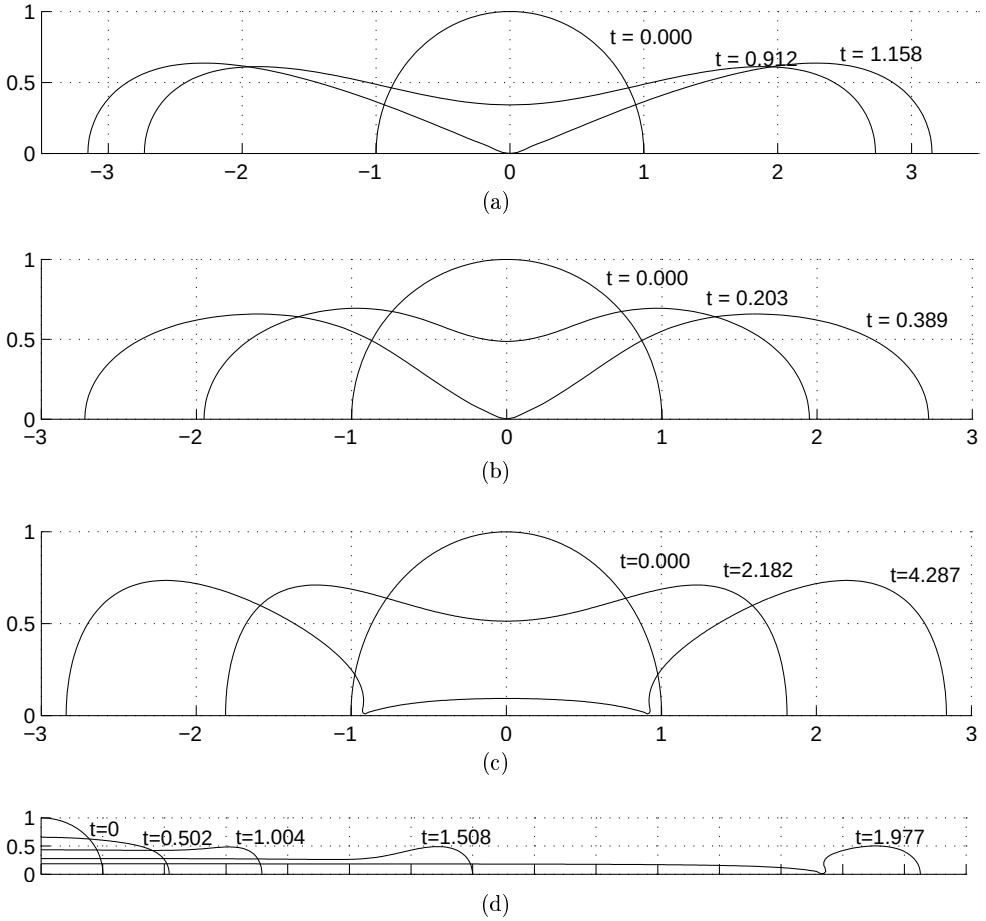

Fig. 2: Time evolution of the break-up process of a drop/bubble for different values of the Weber number. (a) $We = 3.0$ and $\Lambda = 0$, (b) $We = 10.0$ and $\Lambda = 0$, (c) $We = 3.0$ and $\Lambda = 0.8$, (d) $We = 10.0$ and $\Lambda = 0.8$. In this last case, only half of the droplet is shown.

field at scales of the order of the size of the bubble may be considered as homogeneous and isotropic. Consequently, the appropriate time scale for the outer velocity field is the one given by $t_{\Delta u} = \beta^{-1/2}(\varepsilon a_0^{-2})^{-1/3}$, where ε is the dissipation rate of turbulent kinetic energy per unit mass and β is a numerical constant of order unity. Therefore, the turbulent Weber number is usually defined as

$$We_{\rm t} = \frac{\rho_{\rm e}\,\beta\,\varepsilon^{2/3} a_0^{5/3}}{\sigma}, \tag{8}$$

The comparison between the experimentally measured break-up frequency, g, reported in [9] and that provided by the model is shown in Fig.3b. The solid line corresponds to the numerical results which, in order to be appropriately compared with the experimental measurements, need to be scaled as $g = C/(t_c\, T_{\rm b})$ with $C = 0.1$ and $\beta = 5$ for a turbulent critical Weber number $We_{\rm tc} = 2.3$. These proportionality constants account for the degree of freedom involved in the definition of the convective and capillary times. Notice that the numerical computations compare fairly well with experiments even in the case of moderate Weber numbers. Thus, if a Weber number for the problem is defined consistently, the bubble break-up time can be determined by means of this simple model, what avoids to consider more complex aspects of the flow.

DROP BREAK-UP

Numerical results describing the breakup of drops are presented in this section for a wide range of the Weber numbers, We, and density ratios [$\Lambda \sim O(1)$]. The main feature characterizing the droplet break-up process is that, as depicted in Figs. 2c-d, two drops are symmetrically formed at the end sides of an intermediate ligament. Consequently, instead of the binary breakup observed in the case of bubbles, droplets exhibit tertiary break-up. Moreover, the length of the ligament increases with respect to that of the end drops as the Weber number and the density ratio increases. Notice in Fig. 2c that, for values of the Weber number close to the critical one, a small satellite is formed. However, for larger values of the Weber number, the drop elongates considerably, generating a slender ligament whose length, l, is much larger than its radius, a, at the pinch-off time, $l/a \gg 1$, (see Fig. 2d).

The same type of qualitative behavior is experimentally observed in the turbulent breakup of drops at high Reynolds numbers [2]. Note in Fig. 1b that the particle is stretched by the surrounding flow until it is sufficiently elongated to

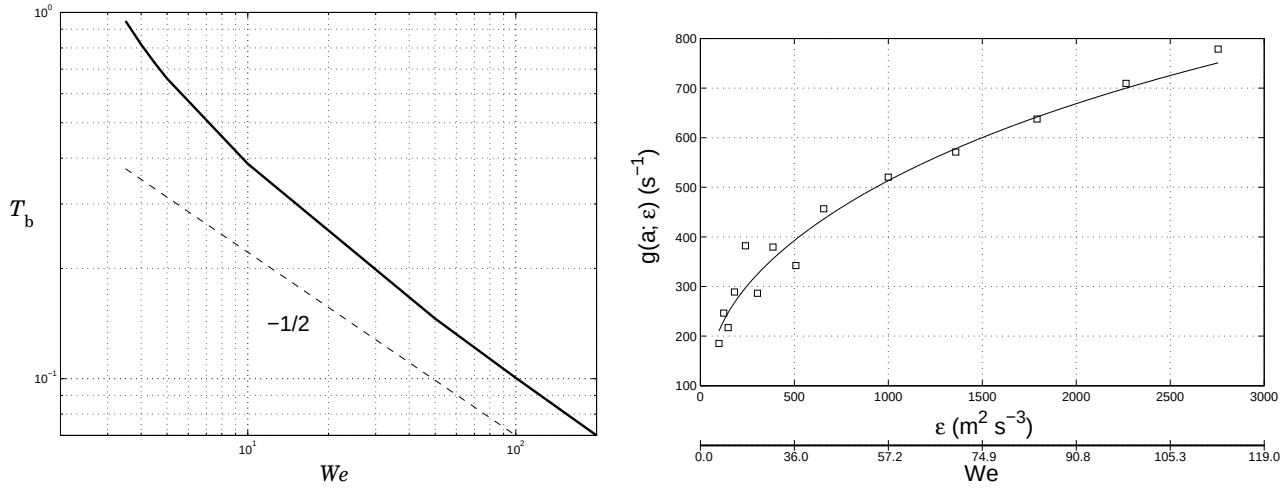

Fig. 3: (a) Dependence of the dimensionless break-up time of bubbles, $T_{\rm b}$, with the Weber number. (b) Comparison of the predicted break-up frequency (solid line) with the experimental measurements of Martínez-Bazán and co-workers [9] (squares) for air bubbles of radius $a \approx 0.89$ mm injected at the axis of a submerged water jet.

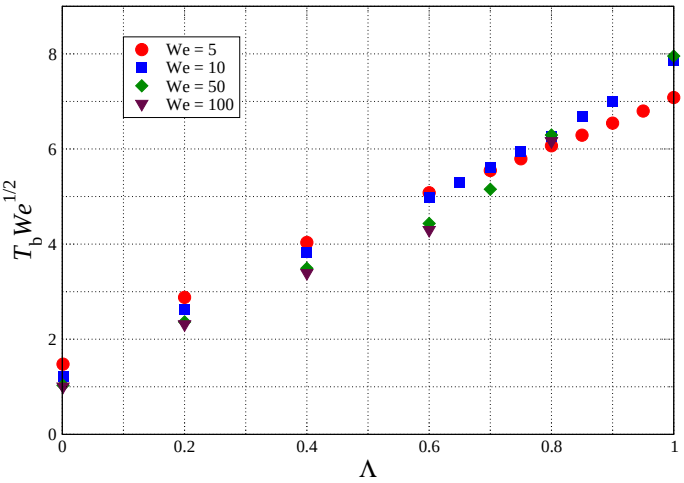

Fig. 4: Dependence of the break-up, $T_{\rm b} We^{1/2}$, with the density ratio Λ for several values of the Weber number.

develop a capillary pinch-off near the tips. The similitude between experimental and numerical observations lead us to the conclusion that the elongation and subsequent break-up of the drop are phenomena driven by inertial and surface tension forces. Thus, although viscous diffusion may influence the breakup frequency [2], the large elongations of the droplets observed in experiments can be attributed to the inner fluid inertia.

The dependence of the breakup time, T_b, on the We and Λ can be also determined from our numerical simulations. Thus, figure 4 shows the scaled breakup time $T_{\rm b}\, We^{1/2}$ as a function of the density ratio Λ. The good collapse of all the data is again a consequence of the fact that the relevant time scale of the problem for sufficiently high values of the Weber number is the convective time. Furthermore, figure 4 also shows that the scaled breakup time depends linearly on the density ratio for $We \gg 1$. This scaling dependence does not follow directly from the analysis but can be justified through a simplified analytical model based on the highly elongated shape of the drop before breaking-up when $We \gg 1$ and $\Lambda \sim O(1)$. This will be the matter of the following subsection.

Description of the evolution of the particle surface when $We \gg 1$ and $\Lambda \sim O(1)$

Fig.2d. shows that, after a short initial transient, the drop deforms into a slender ligament with a slowly varying diameter except in a region close to the ends. This suggests that, during most of the break-up process, the drop may be modelled as a constant volume cylinder whose radius and length (a and l respectively) are time dependent. The first order solution ($l/a \to \infty$) for the velocity field inside and outside the cylinder can be analytical obtained by solving the Laplace equations (2) together with the boundary conditions given by equations (4), (5) and (7). Moreover, since the model assumes that the ligament is a cylinder, the normal stress balance condition (6) can be conveniently written as

$$p_{\rm i}\left(r=a,z,t\right) - p_{\rm e}\left(r=a,z,t\right) = \frac{1}{a(t)}\,, \tag{9}$$

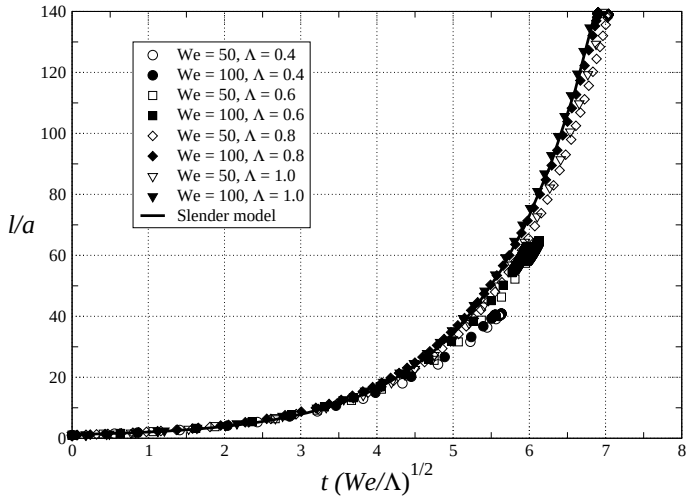

Fig. 5: Time evolution of the ligament's aspect ratio obtained from numerical simulations for different values of Λ and We together with the evolution predicted by Eq. (10).

Hence, once the condition (9) is imposed at the ligament's interface, a free parameter equation governing the time evolution of $a(t)$ can be written in terms of the scaled variable $T = t\sqrt{We/\Lambda}$ as,

$$\frac{\ddot{a}}{a} - 3\frac{\dot{a}^2}{a^2} + \frac{1}{8} = 0\,, \tag{10}$$

This simple model has been validated by comparing the time evolution of the drop aspect ratio l/a predicted by (10) together with the mass conservation equation ($l\,a^2 = \text{constant}$), with the results obtained numerically. Fig. 5 shows that the numerical results, obtained for a wide range of We and Λ values, follow very closely the $l/a(T)$ function given by equation (10). However, it must be also noticed that the numerical results deviate from the model for density ratios $\Lambda \leq 0.4$. Such deviation is due to the fact that the slenderness hypothesis is no longer satisfied.

The result shown in Fig.5 also indicates that the stretching time scales with the square root of the density ratio. Consequently, the stretching process has a different time dependence with Λ than the breakup process previously described (see Fig.4). This different trend can be explained by noticing that the break-up process may be divided into two separated stages: an inertial one, in which the drop stretches in the way explained above, and a capillary driven pinch-off, similar to that described in [11].

Since the second stage is much shorter than the first one, the break-up time may be assumed to be the time taken by the drop to reach a transition radius, $r_{\rm tran}$, below which inertial effects are no longer important. Our Simulations showed that this transition radius depends only on the density ratio. Hence, taken the asymptotic limit of Eq. (10) for long times, the break-up time may be estimated as

$$t_{\rm b} \sim -\sqrt{\Lambda/We}\,\log r_{\rm tran}(\Lambda) \tag{11}$$

Therefore, the break-up time grows faster than the square root of the density ratio since, in the range of parameters considered here, $r_{\rm tran}$ decreases monotonically with Λ.

CONCLUSIONS

The main features of the break-up of a drop or bubble in an homogeneous and isotropic turbulent flow have been reproduced under the potential flow approximation, assuming that the flow pattern producing the breakup is an axisymmetric hyperbolic type of flow described by [3]. In the case of bubbles, the break-up time predicted by the numerical model agrees very well with that experimentally measured by [9, 10] once the Weber number is properly defined.

The role of the inner fluid density in the break-up process has also been investigated. A first result of interest, which agrees with experimental observations [2], is that, if the inner and outer fluid densities are comparable, the drop deforms into a slender ligament and ultimately breaks-up due to capillary pinch-off. Furthermore, since viscous diffusion is not included in the model, it can be concluded that the break-up process is driven by inertia forces. In addition, a simple analytical model that accurately reproduces the numerically obtained time evolution of the drops radii in the cases of $We \gg 1$ and $\Lambda \sim O(1)$ has also been developed .

This research has been supported by the Fifth Framework Programme of the European Commission under the Energy, Environment and Sustainable Development Contract No. EVG1-CT-2001-00042 EXPRO and by the Spanish MCyT under Project No. DPI2002-04550-C07-06.

LIST OF SYMBOLS

a_0	Initial radius of the particle.	$t_{\Delta \mathrm{u}}, t_{\mathrm{c}}$	Convective and capillary times.
a	Dimensionless radius of the ligament.	$u_{(r,z)}$	Velocity components.
g	Break-up rate of bubbles.	We	Weber number.
l	Dimensionless ligament length.	Δu	Velocity difference between the poles at $t = 0$.
M	Intensity of the straining flow.	ε	Dissipation rate of turbulent kinetic energy.
$\mathbf{n}_{(\mathrm{i,e})}$	Normal vector to the interface.	$\phi_{(\mathrm{i,e})}$	Dimensionless inner and outer velocity potentials.
$p_{(\mathrm{i,e})}$	Inner and outer dimensionless pressures.	Λ	Density ratio between the inner and outer fluids.
r_{tran}	Dimensionless transition radius.	$\rho_{(\mathrm{i,e})}$	Inner and outer densities.
$t_{\mathrm{b}}, T_{\mathrm{b}}$	Dimensional/Dimensionless break-up time.	σ	Surface tension coefficient.

REFERENCES

1. J. Rodríguez-Rodríguez, C. Martínez-Bazán and J.L. Montañés. A novel particle tracking and break-up detection algorithm: application to the turbulent break-up of bubbles. *Measurement Science and Technology*, vol.14, pp. 1328-1340, 2003.
2. C.D. Eastwood, L. Armi and J.C. Lasheras. The break-up of immiscible fluids in turbulent flows. *Journal of Fluid Mechanics*, vol.502, pp 309-333, 2004.
3. J.O. Hinze. Fundamentals of the hydrodynamics mechanisms of splitting in dispersion process. *AIChE Journal*, vol.1, pp. 289-295, 1955.
4. H.A. Stone. Dynamics of drop deformation and breakup in viscous fluids. *Annu. Rev. Fluid Mech.*, vol.26, pp 65-102, 1994.
5. R. Shreekumar, R. Kumar and K.S. Gandhi. Breakage of a drop of inviscid fluid due to a pressure fluctuation at its surface. *Journal of Fluid Mechanics*, vol.328, pp 1-17, 1996.
6. F.J. Higuera. Axisymmetric inviscid interaction of a bubble and a vortex ring. *Physics of Fluids*, vol.16, pp 1156-1159, 2004.
7. J. Rodríguez-Rodríguez, C. Martínez-Bazán and J.M. Gordillo. Break-up of a drop or bubble at high Reynolds number. *In preparation*.
8. F. Risso and J. Fabre. Oscillations and breakup of a bubble immersed in a turbulent field. Journal of Fluid Mechanics, Vol 372, pp 323-355, 1998.
9. C. Martínez-Bazán, J.L. Montañes and J.C. Lasheras. On the breakup of an air bubble injected into a fully developed turbulent flow. Part I: Breakup frequency. *Journal of Fluid Mechanics*, vol.401, pp. 157-182, 1999.
10. C. Martínez-Bazán, J.L. Montañes and J.C. Lasheras. On the breakup of an air bubble injected into a fully developed turbulent flow. Part II: Size pdf of the resulting daughter bubbles. *Journal of Fluid Mechanics*, vol.401, pp. 183-207, 1999.
11. D. Leppinen & J.R. Lister. Capillary pinch-off in inviscid fluids. *Phys. of Fluids* vol.15, pp. 568-578, 2003.